Reduction of Transfer Threshold Energy for Laser-Induced Jetting of Liquids using Faraday Waves

Emre Turkoz,[1] SeungYeon Kang,[1] Xiaohan Du,[1] Luc Deike,[1,2] and Craig B. Arnold[1,*]

[1] *Department of Mechanical and Aerospace Engineering, Princeton University, Princeton, NJ 08544, USA*
[2] *Princeton Environmental Institute, Princeton University, Princeton, NJ 08544, USA*

(Received 3 January 2019; revised manuscript received 14 March 2019; published 8 May 2019)

Flow-focusing is used in microfluidics to generate droplets that are smaller than the characteristic length scale of the flow geometry. Conventionally, flow-focusing takes place inside micrometer-sized channels due to capillary effects. In this study, we demonstrate that the transient meniscus profile created with Faraday waves on liquid films can enable flow-focusing. Using a magnetic shaker, we generate Faraday waves on a liquid film leading to flow-focusing that increases the resolution of a nozzleless, jet-based printing technique called blister-actuated laser-induced forward transfer (BALIFT). We perform experiments to demonstrate how transient meniscus formation enables jetting at lower laser-pulse energies than the threshold, and use numerical modeling to examine this process at smaller length scales relevant to printing applications.

DOI: 10.1103/PhysRevApplied.11.054022

I. INTRODUCTION

Flow-focusing is a well-known phenomenon in microfluidics used to create small droplets within micrometer-sized channels [1,2]. Recently, this phenomenon has been shown to result in very fast and thin jets from capillary tubes using a pressure impulse such as the absorption of a laser pulse [3] or the mechanical impact resulting from a coil gun [4]. Flow-focusing has also been integrated into inkjet printing to print highly viscous fluids from capillary tubes [5] and into blister-actuated laser-induced forward transfer (BALIFT) [6], which is the method used in this study to generate liquid jets, to reduce the ejected droplet size by half.

In these conventional applications of flow-focusing, the liquid forms a steady meniscus profile at the liquid-air interface due to surface tension. The desired profile is created by adjusting the geometry in order for the surface-tension effects to be enhanced. In this study, we use a new approach and create a transient meniscus profile on a liquid-thin-film surface to generate focused jets. This is achieved by generating Faraday waves [7] into a liquid thin film using a magnetic shaker. We use the BALIFT technique to create jets by directing the laser pulse onto the surface points corresponding to the trough of the Faraday wave on the liquid film. We investigate the resulting focused jets using both experimental and numerical techniques to compare with the results from the regular jets induced from a flat liquid film.

BALIFT is a nozzleless jet-based deposition technique where the energy of a laser pulse is converted into mechanical energy through a rapidly expanding blister on a solid thick film [8]. With a liquid layer coating the polymer layer, this rapid blister expansion provides the impulsive pressure gradient [9] for jet formation and material transfer. By forcing Faraday waves into the liquid film, we exploit the geometrical effect of the meniscus-shaped interface, so that the focused laser pulse leads to the formation of a focused jet.

Faraday waves are induced by vibrating a liquid container perpendicular to the liquid-air interface above a certain acceleration threshold for a given set of parameters including liquid density ρ_l, liquid dynamic viscosity μ_l, liquid-air surface tension γ, and thickness of the liquid film H_f [10–12]. For our experiments, we work close to the instability threshold, and obtain a regular wave pattern with a wavelength corresponding at half the forcing frequency. The relationship between the wavelength and the frequency is given by the dispersion relation for gravity-capillary waves with a depth H_f,

$$\omega^2 = \tanh\left(kH_f\right)\left(\frac{\gamma}{\rho_l}k^3 + gk\right), \tag{1}$$

where ω is the angular frequency, $k = 2\pi/\lambda$ is the wave number, and g is the gravitational constant.

In this article, we first show experimentally that Faraday waves make jetting possible for subthreshold laser energies. We perform the experiments for relatively large liquid-film thicknesses compared to conventional LIFT printing applications due to experimental limitations in

*cbarnold@princeton.edu

generating Faraday waves with an electromagnetic shaker. We show experimentally that Faraday waves reduce the laser-transfer threshold energy. To demonstrate the applicability of this technique for small length scales, we perform direct numerical simulations. We validate our numerical model for small and large liquid-film thicknesses. Our results show that Faraday waves can lead to the ejection of smaller droplets and therefore increase the resolution of the printing process.

II. EXPERIMENTS

The simplified schematic of our experimental setup is presented in Fig. 1(a). A 7-μm-thick polyimide film is coated on a glass slide via spin coating. The liquid film [deionized water with 0.1 wt % Triton X-100 surfactant (surface tension $\gamma = 30.4$ mN/m, liquid dynamic viscosity $\mu = 0.89$ Pa s)] is coated by injecting the desired volume onto the sample and using a magnetic shaker at low frequencies and amplitudes to spread the drop uniformly as a thick film. For the data presented in this study, the film thickness is $H_f \approx 160$ μm. The laser spot size is approximately equal to 30 μm and the pulse energy is measured as 138 ± 1.7 μJ. The imaging of the resulting flow field is performed using a high-speed camera (Phantom v2012) with a macro lens (Nikon 200 mm f/4 AF-D) and an LED backlight. The substrate coated with the liquid film is oscillated vertically at 100 Hz using a magnetic shaker (Bruel & Kjaer LDS V455). The resulting Faraday waves are imaged with a slight angle as presented in Fig. 1(b).

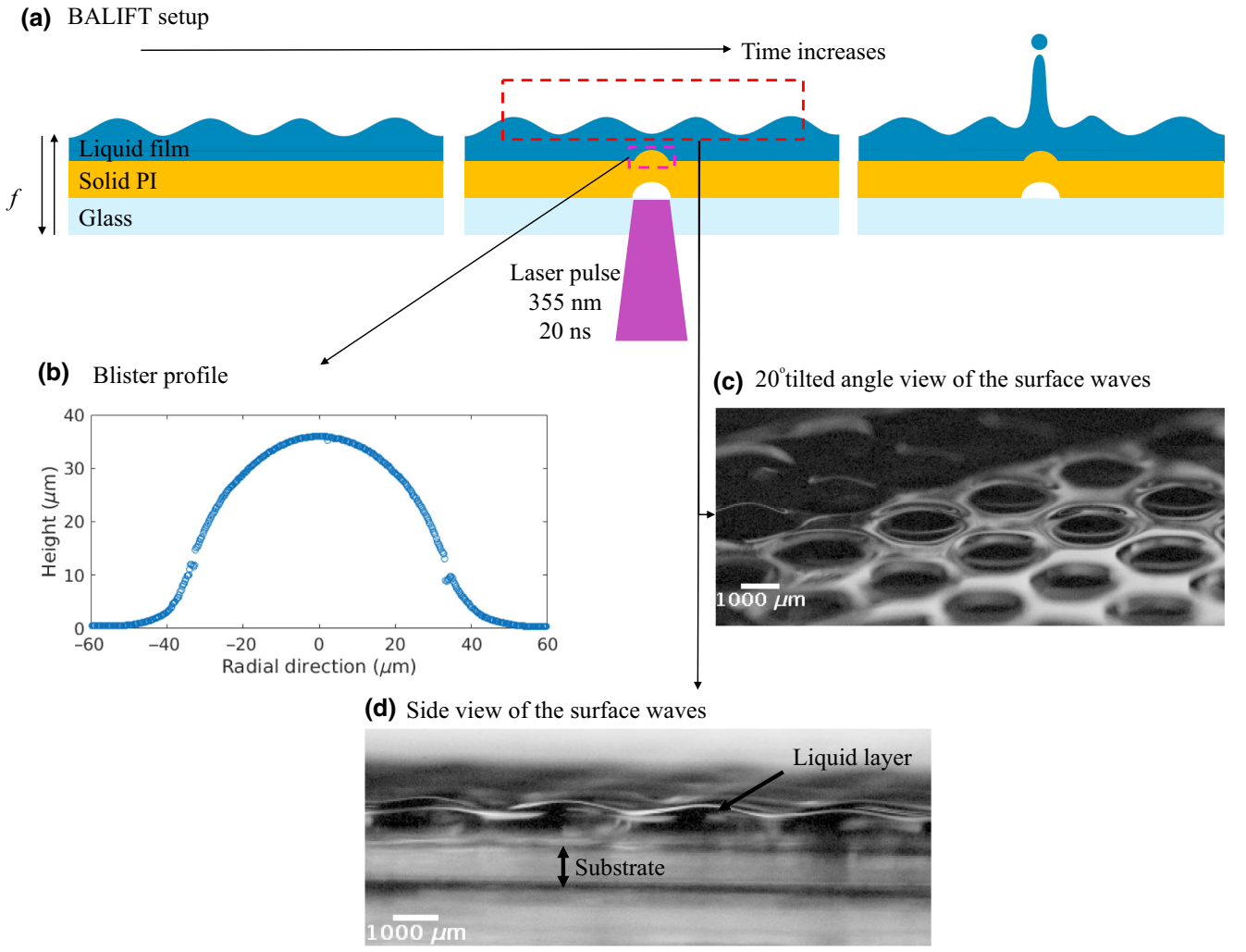

FIG. 1. The Faraday-wave transient meniscus is coupled with the energy of the laser pulse to deposit materials. (a) Schematic of the experimental setup. The liquid film is coated on a solid polyimide 7-μm-thick film deposited on a transparent glass slide. We oscillate the substrate using a magnetic shaker. When the instability is generated with an acceleration above the critical value, we observe Faraday waves on the liquid surface. The laser pulse is then directed to the lowest point of the trough at the right time. (b) Dimensions of the blister measured using confocal microscopy. (c) The camera image of surface Faraday waves of a 160-μm deionized water layer on polyimide film from a 20° tilted angle. The magnetic shaker frequency is set to 100 Hz. (d) Side images of the Faraday standing waves, which are used as the transient meniscus for the BALIFT process.

The resulting Faraday waves have a wavelength of approximately 3.1 mm, in agreement with the dispersion relation (1), and an amplitude of approximately 80 μm. Therefore, below the trough of the wave, the minimum ink thickness is 80 μm while it is 240 μm at the crest. For the flow-focusing to take place, it is crucial to synchronize the laser pulse to hit the trough of the wave when its amplitude is at a maximum. This is done using a pulse generator so the laser pulse is sent at the right time corresponding to the end of each period. To demonstrate that Faraday waves lower the transfer threshold energy, we present the images from a high-speed video of a transfer experiment. For the flat-film case, the laser pulse does not deposit enough energy to the fluid and the resulting fluid motion does not yield jet formation as shown in Fig. 2. On the other hand, when we introduce Faraday waves, we see from Fig. 3 that the resulting jet breaks up into droplets. In this figure, at $t = t_0$, we see the reflection of the plasma created by the absorption of the laser pulse by the polyimide layer [13]. As time progresses by $t = t_0 + 750$ μs, we see the breakup of the first droplet from the jet. At $t = t_0 + 1500$ μs, we see the second droplet that retracts back to the liquid film. As a result, the resulting jet breaks up into two droplets while one of the droplets is ejected away from the thin-film surface and the other one goes back to the thin film. The ejected droplet has the approximate radius of 67 μm.

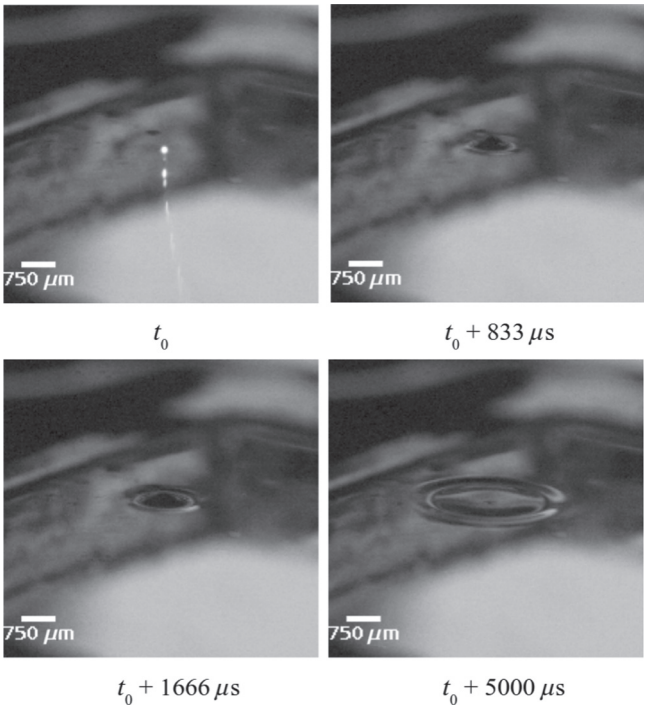

FIG. 2. Snapshots of the video for the flat-film case. The plasma formed during the absorption of the laser pulse by the polyimide layer is apparent at the first snapshot denoted with t_0. The formed jet does not result in breakup.

As shown in Fig. 3, Faraday waves make it possible for the jetting to take place at subthreshold energies as observed previously with the steady meniscus configuration [6]. However, the question remains whether this improvement is due to a simple effective thickness reduction or whether flow-focusing is playing a role as well. To answer this question and test this phenomenon at thinner liquid films, we perform numerical simulations of the BALIFT process. For instance, previous applications of BALIFT deal with the typical film thickness values on the

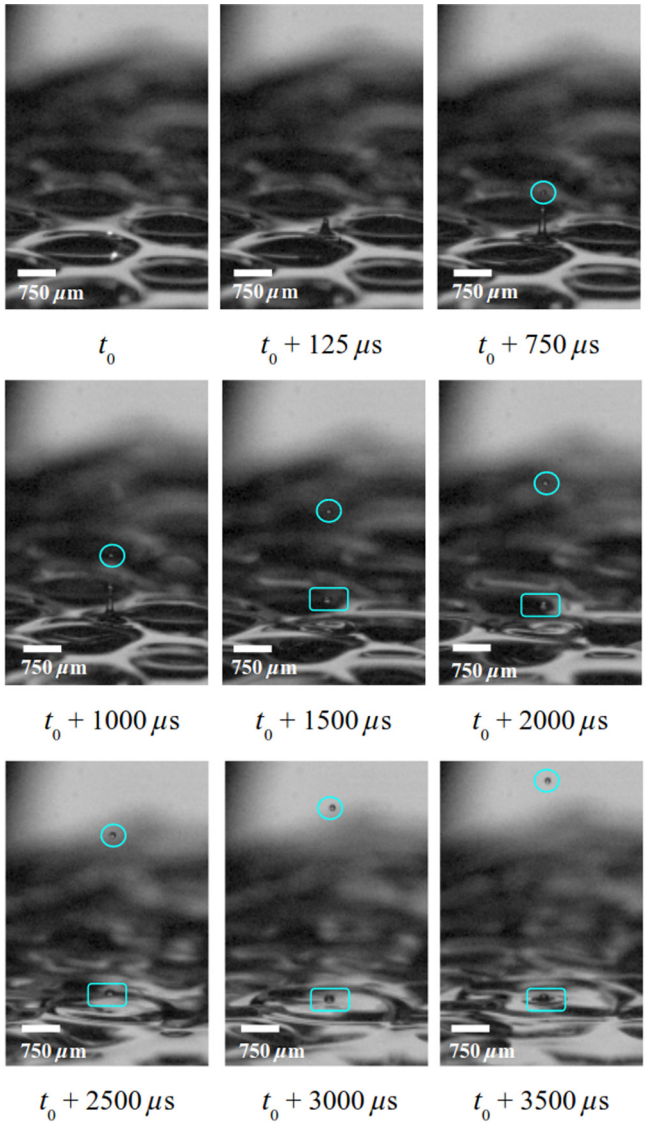

FIG. 3. Images from videos of the BALIFT process. The liquid-layer thickness is 160 μm. The laser-pulse energy and spot size are the same as in the flat-film case. The videos are taken with 200 000 frames/s. t_0 denotes the time when the laser pulse is sent to the sample. The jetting is possible with Faraday waves. The magnetic shaker frequency is 100 Hz. The resulting jet breaks up into multiple droplets. The blue circle on each figure points out the droplet ejected while the blue rectangle shows the droplet retracting back to the liquid film.

order of approximately 5 μm [9,14]. Such small thickness values are preferred for printing because the ejected droplet size from liquid films is proportional to the film thickness value [15].

III. NUMERICAL SIMULATIONS AND VALIDATION

We solve the axisymmetric two-phase incompressible Navier-Stokes equations with surface tension using the open source flow solver BASILISK [16,17]. With this solver, the interface between the liquid layer and the ambient air is captured by a volume-of-fluid (VOF) method. These methods have been previously validated for various complex multiphase problems including splashing [18], breaking waves [19], bubble bursting [20], thinning of viscoelastic liquid bridges [21], and also the breakup of jets induced by BALIFT [22].

One of the most crucial parts of the model is the implementation of the boundary deformation during blister formation. The time-dependent blister profile δ is given by [14] as $\delta(r,E,t) = X(r,E)T(t)$, where $X(r,E)$ and $T(t)$ define the energy-dependent (E in μJ) blister profile and the time-dependence function, respectively. The blister profile is expressed as $X(r,E) = H_0(E)\{1-[r/R_b(E)]^2\}^C$ (in μm) and the time-dependence function is expressed as $T(t) = (2/\pi)\arctan(t/\tau_b)$, where $H_0(E) = -0.0093E^2 + 2.5708E - 9.2618$ is the laser energy-dependent blister height (in μm), $R_0(E) = 18.117\ln(E) - 12.887$ is the blister radius (in μm), C is a shape coefficient, and $\tau_b = 23.5\times10^{-9}$ s is the characteristic time scale for blister formation [23] for the 20-ns pulse laser used in this study.

The jetting and breakup of a liquid jet depend on the ambient air properties as well [24]. In addition to the blister deformation, the problem is governed by the dimensionless parameters μ_a/μ_l, ρ_a/ρ_l, τ_b/t_c, and the Ohnesorge number $\mathrm{Oh} = \mu_l/\sqrt{\rho_l\gamma H_f}$, where $t_c = \sqrt{\rho_l H_f^3/\gamma}$ and subscript a denotes the corresponding parameters of air.

We first present the snapshots from the simulation results for a flat film of 5 μm with the laser-pulse energy of 5.14 μJ in Figs. 4(a)–4(d) obtained from simulations performed with the refinement approximately corresponding to 10.68 cells/μm resolution. We evaluate the blister height and radius with the formulas given above as $H_0 = 3.7$ μm and $R_0 = 16.8$ μm, respectively. The transferred droplet volume at this threshold energy is evaluated with increasing grid resolution. This result is presented in Fig. 4(e). The grid convergence study is performed with an adaptive grid on a single node and multiple processors with message passing interface (MPI) parallelization. Figure 4(e) shows that all of the cases converge numerically for the mesh size above 10 cells/μm.

We then validate our numerical simulations in the flat-film case by comparing the numerical results with the experimental results and previous computational work

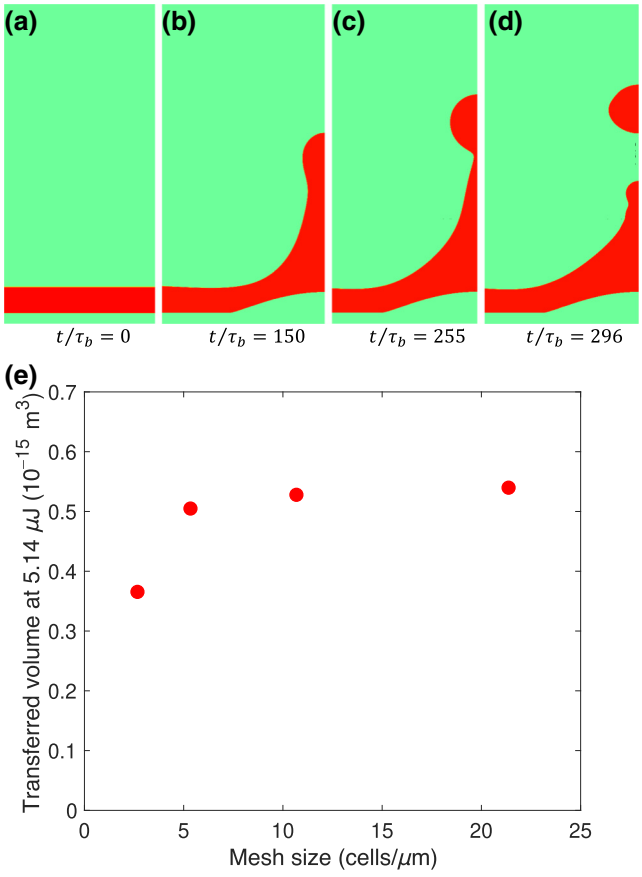

FIG. 4. Grid convergence of the numerical model implemented in the BASILISK open source flow solver for the flat-film case. (a)–(d) The snapshots obtained from simulations performed with the refinement corresponding to 10.68 cells/μm refinement. (e) The grid convergence study is performed for an adaptive grid with MPI parallelization on multiple modes and processors. Transferred droplet volume converges above 10 cells/μm.

[14]. Figure 5 shows the ejected droplet volume from our BASILISK simulations, which reproduce the experimental data and earlier modeling results with great accuracy.

The validation presented in Figs. 4 and 5 is for a liquid film of thickness 5 μm. Now, we test the validity of the numerical model with thicker films such as those used in the experiments described in Sec. II. To test the validity of the model for large ink thicknesses, we compare the numerical results with the experimental images of the BALIFT process with a 65-μm-thick liquid film of a water-glycerol solution (80 wt % water and 20 wt % glycerol) with 0.1 wt % Triton X-100 surfactant ($\mu = 1.7$ mPa s, $\gamma = 30.4$ mN/m). We use the same laser-pulse energy that creates the blister profile presented in Fig. 1(b), where $H_0(E) = 38$ μm, $R_0(E) = 50$ μm, and the shape factor $C = 2.73$. We note that the grid convergence study is performed for this configuration as well and the same resolution as the previous case (approximately 10 *cells*/μm) is employed. The grid refinement used in the previous

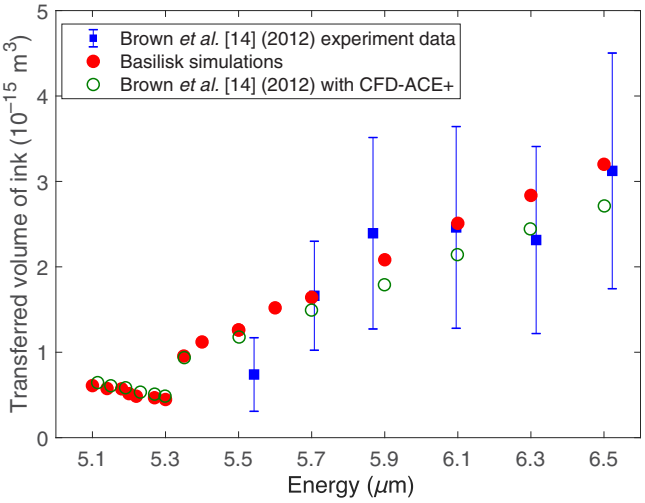

FIG. 5. Validation of the numerical results with the experiments. We observe that BASILISK simulations produce results that are within the standard deviation of the experimental results and in good agreement with the modeling presented in [14].

section also yields numerically converged results for this configuration.

Results of the jet formation from both the experiment and simulation are presented in Fig. 6. For these high-speed videos, we used the same high-speed camera with a microscope (InfiniTube with a Mitutoyo $\times 10$ objective) for higher resolution. It is seen from the high-speed video images that, even though initially the numerical jet is shorter, the features of the jet are very similar for both jets. While the experimental images show an elongated neck right before droplet breakup as seen in Figs. 6(b) and 6(c), the neck is shorter for the simulated case. The ejected droplet has a diameter of 38.8 μm as measured from the images. The simulations yield a droplet diameter of 36.8 μm, which is very close to the experimentally obtained value.

High-speed videos allow us to record the length of the jet measured from the surface at each time step. The evolution of jet length as a function of time from the experiment and the numerical simulation is presented in Fig. 6(e). While the simulation results do not follow the experimental curve exactly, they succeed in representing the main features of the jet. According to the simulations, the breakup takes place at $t = 44.6$ μs, which is very close to the experimentally obtained value of $t \approx 48.5$ μs. We note that while the simulations predict the droplet size and time of breakup in very good agreement with the laboratory experiments, the jet dynamics presented in Fig. 6(e) exhibit some differences. These differences are likely to be due to the formulation of the solid boundary deformation. The time dependence of the blister profile presented in our previous work [14] and used here assumes that the blister expands monotonically while we showed in our previous studies

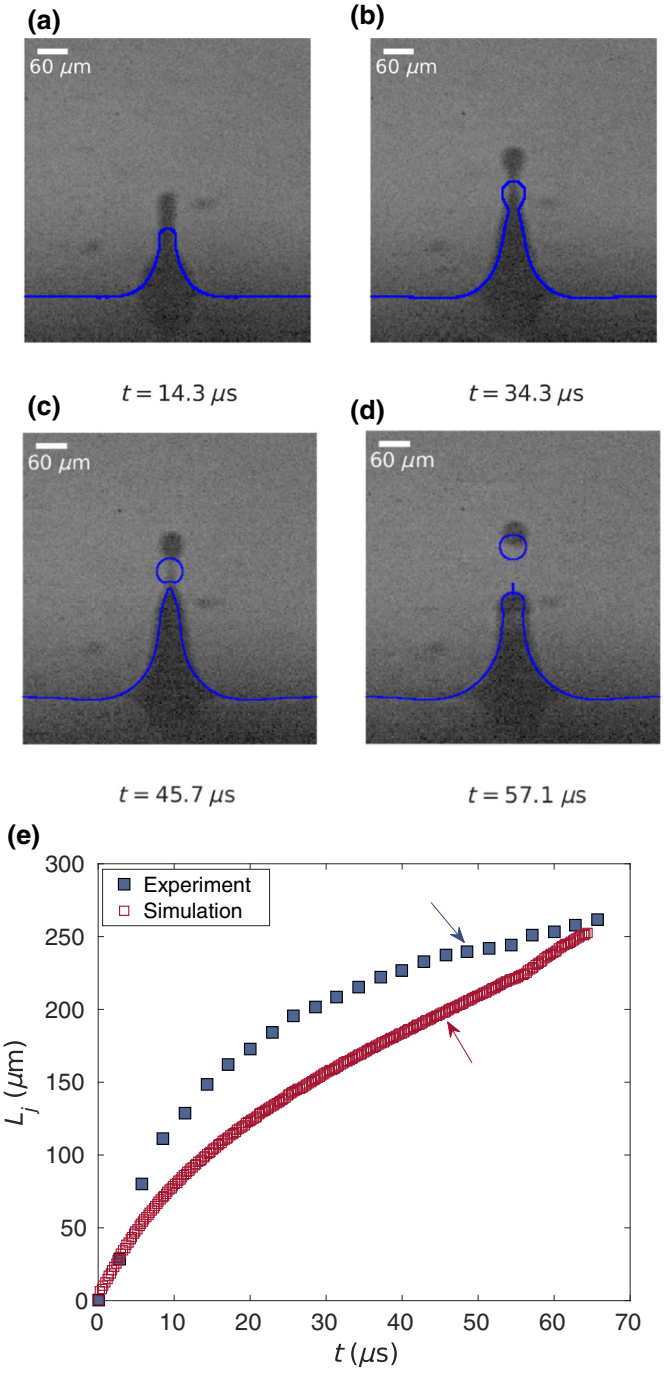

FIG. 6. Validation of the numerical model with high-speed video images of experiments. (a)–(d) Superposition of experimental and numerical profiles. The ejected droplet diameter from the simulations is 36.8 μm, which is very close to the experimental value of 38.8 μm. (e) Jet length L_j as a function of time t obtained from experiments and simulations for the same configuration as presented in (a)–(d). The colored arrows indicate the moment of breakup for each case.

[13] that the blister height and volume exhibit oscillations after the blister reaches its full length. Furthermore, the shape of the blister also changes dynamically during the

expansion (during the first approximately 25 ns), where the blister initially has a pointed tip that then relaxes to a Gaussian profile. Experiments and numerical simulations of jetting in other contexts have demonstrated an extreme sensitivity in the geometry of the focusing process leading to the jet formation [20,25], so that the uncertainties in the blister dynamics directly affect the resulting liquid jet dynamics.

This completes the validation of the numerical model developed for this study. We note that there are no fitting parameters for the direct numerical simulations, and the results from the numerical model show good agreement with the experiments.

IV. RESULTS

Now, we simulate the effect of Faraday waves at small length scales relevant to printing applications. We consider Faraday waves with wavelength $\lambda_c = 150\ \mu$m. To represent the Faraday waves in our model, we represent the surface profile as an axially symmetric sinusoidal function that can be formulated as $H_f + a\cos[(2\pi/\lambda_c)(\lambda_c/2 - r)]$, where a is the wave amplitude, r is the radial coordinate, and $H_f = 5\ \mu$m is the average film thickness value we picked in accordance with previous applications [9,14]. This sinusoidal shape assumed for the Faraday waves matches the solutions of the governing equations and wave patterns that are experimentally observed in the literature [10,26,27]. Note that the wave simulated in this section has very similar depth-to-wavelength ratio to that considered for the thick film in Sec. II, where $H_f/\lambda = 0.05$ for the thick film and $H_f/\lambda_c = 0.033$ for the thin film in this section. So in both cases we are in an intermediate-depth configuration. We only consider the geometrical effect of Faraday waves because the wave dynamics takes place at a time scale much slower than the laser-induced blister formation, $1/\omega \gg \tau_b$. The minimum thickness value along the wave profile corresponds to $r = 0$ with $H_{\min} = H_f - a$. We sweep different Faraday-wave amplitudes from 0.5 to 2.5 μm. We picked $a = 2.5\ \mu$m as the largest amplitude as this value satisfies the criterion $a/\lambda_c < 0.1$, which as we experimentally observed leads to spatially stable Faraday waves.

An example of the jet dynamics and the jet profiles is presented in Fig. 7. In this figure, the flat-film case $a = 0.0\ \mu$m at the transfer threshold energy $E_{\text{th}} = 5.09\ \mu$J, shown in blue, is presented with the Faraday-wave case $a = 2.5\ \mu$m at a lower laser-pulse energy of $E = 4.95\ \mu$J, shown in red. For each of these cases, the black curve at the bottom denotes the interface between the liquid film and the solid polyimide layer, and the colored curve at the top denotes the interface between the liquid film and air. Figure 7(a) shows the initial case where the liquid-solid interface is flat and the blister formation is yet to take place. After blisters form [Figs. 7(a) and 7(b)], the liquid films

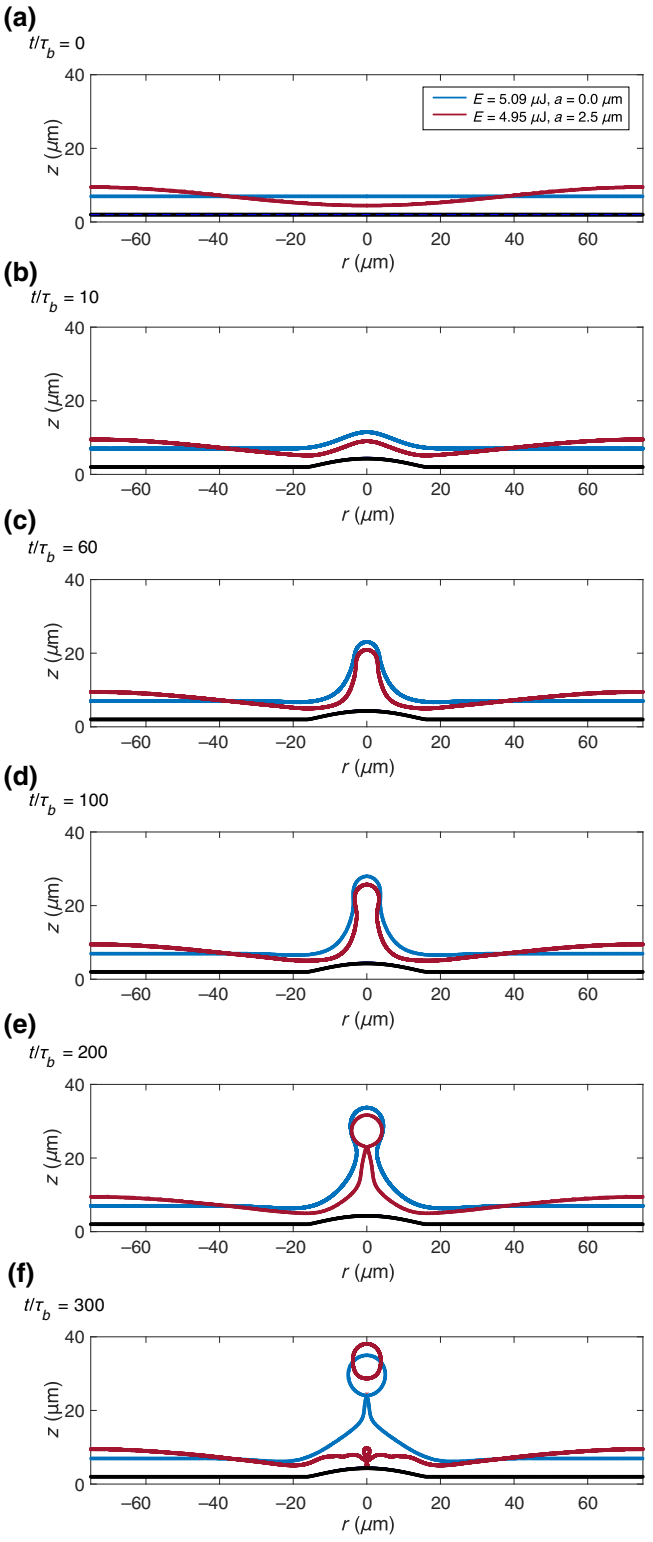

FIG. 7. Snapshots of the jet profiles from numerical simulations. Blue curves represent the flat-film case ($E = 5.09\ \mu$J) while red curves represent the case with $a = 2.5\ \mu$m Faraday-wave amplitude ($E = 4.95\ \mu$J). The two black profiles at the bottom denote the interface between the liquid and the blister while the two colored profiles at the top represent the interface between the liquid and air.

yield jet formation that results in breakup [Figs. 7(c)–7(f)]. We see from this figure that the droplet ejected using Faraday waves is smaller and faster compared to that ejected from the flat film [Figs. 7(e) and 7(f)].

Figure 8 shows results for the Faraday-wave configurations for increasing laser-pulse energy and increasing wave amplitude. While the filled symbols denote single drop ejections per laser pulse, the open symbols represent the multiple drop cases. Ejecting a single drop per pulse is the preferred method for printing, and the lowest deposited droplet volume is obtained at the transition from single drop to multiple drop regimes [14]. This corresponds to 5.22 μJ for the no-Faraday-wave ($a = 0$ μm) case with an ejected droplet size of 4.72 μm. However, when a Faraday wave of amplitude $a = 2.5$ μm is introduced into the system, the resulting configuration with the minimum film thickness $H_{\min} = 2.5$ μm results in a smaller droplet with a radius of 4.04 μm with a 5.02 μJ laser pulse. This means that Faraday waves and the resulting flow-focusing effect can achieve approximately 40% reduction of volume, which is close to the 50% improvement we previously demonstrated with steady meniscus formation [6]. The inset presents the reduction in transfer threshold energy as a function of Faraday-wave amplitude in Fig. 8. We see that the threshold energy converges to a value lower than the flat-film threshold energy as the Faraday-wave amplitude is increased.

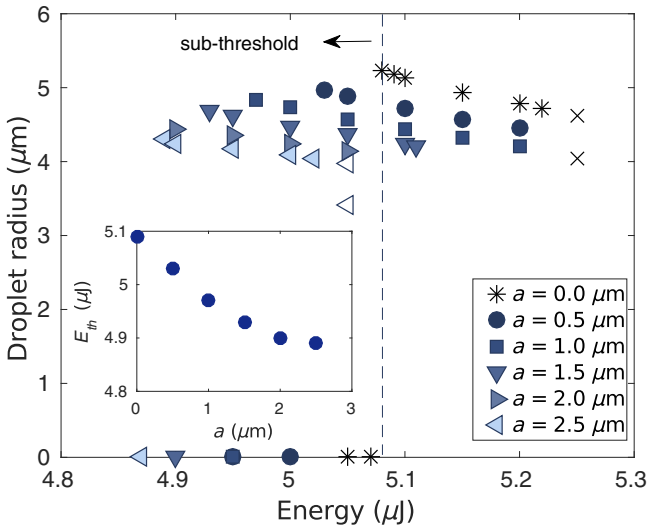

FIG. 8. Results of the BASILISK simulations. The flow-focusing effect due to Faraday waves lowers the transfer threshold laser energy. Filled symbols denote single drop ejections and empty symbols denote multiple-drop ejections. For flat-film cases ($a = 0.0$ μm), the single drop ejections are represented with ($*$) while the multiple-drop case is represented with ($\times$). Single drop ejections obtained using Faraday waves show smaller droplets compared to the no-Faraday-wave case. The inset shows the reduction in transfer threshold energy as a function of the Faraday-wave amplitude.

The average film-thickness value of $H_f = 5$ μm has a transfer threshold energy of 5.09 μJ with no additional Faraday wave as shown in Fig. 8. This threshold energy produces a droplet with a radius of 5.23 μm. We also indicate the threshold laser energy with a vertical dashed line for the no-Faraday-wave case. The introduction of Faraday waves makes it possible for the ejection to take place at lower energies than this threshold energy. Thus, Fig. 8 shows that the creation of a shallow meniscus using Faraday waves improves the process by lowering the threshold energy and ejected droplet size.

V. DISCUSSIONS AND CONCLUSION

We show here that Faraday waves can create meniscus-shaped interfaces and lead to flow-focusing when coupled with an impulsive pressure such as that provided by the BALIFT process. This technique has a major advantage over conventional flow-focusing applications as the formation of the meniscus does not depend on the wettability of the liquid to solid walls. Faraday waves can be generated on liquid thick films without confinement.

It is important to note that the viscous dissipation term can be important for Faraday waves generated using liquids with high viscosity values. The viscous dissipation rate δ for a wave of frequency ω is proportional to $\delta \sim \nu k^2 \omega^{-1}$, where $\nu = \mu/\rho$ is the kinematic viscosity [28,29]. It is still possible to generate Faraday waves with highly viscous liquids; however, a larger acceleration is required to overcome the viscous dissipation as the instability threshold depends on viscosity and frequency [30]. Exciting Faraday waves of 150 μm wavelength would require forcing at approximately 10 000 Hz.

An important aspect of inducing jets with flow-focusing is the determination of the relationship between the ejected droplet size and the relevant parameters. To our knowledge, there is no established theory that relates the droplet size to the meniscus size. The previous literature on flow-focusing [3,31] has focused on the scaling of jet velocity with capillary diameter, pressure gradient, and surface tension. We have experimentally observed that the ejected droplet size decreases as the pressure impulse is increased; however, the resulting jets produce multiple droplets. In addition, numerical simulations, as presented in Fig. 8, indicate that as the amplitude-to-wavelength ratio (a/λ_c) is increased, the ejected droplets are smaller. However, a more systematic study can be performed in the future to see the effect of the wavelength on the ejected droplet size.

In this article, we show experimentally and numerically that Faraday waves enhance the jetting process during BALIFT by lowering the transfer threshold energy and decreasing the ejected droplet radius. Transient meniscus formation leads to flow-focusing as steady meniscus formation does [5,6]. In this study, we couple the geometrical

effects due to the meniscus-shaped interface with the laser energy to print smaller droplets using flow-focusing. We believe that this study will pave the way for the development of new laser jetting techniques that incorporate multiple forms of energy to enhance droplet resolution.

ACKNOWLEDGMENTS

We acknowledge the funding by the National Science Foundation (NSF) through a Materials Research Science and Engineering Center program (Grant No. DMR-1420541). The computations were partially performed using allocation TGOCE140023 to L.D. from the Extreme Science and Engineering Discovery Environment (XSEDE), supported by NSF Grant No. PACI-1053575, and using Princeton Research Computing resources, including the Princeton Institute for Computational Science and Engineering and the High Performance Computing Center. We also acknowledge funding by the Princeton University Schmidt Fund.

[1] A. L. Shelley, N. Bontoux, and H. A. Stone, Formation of dispersions using 'flow focusing' in microchannels, Appl. Phys. Lett. **82**, 364 (2003).
[2] H. A. Stone, A. D. Stroock, and A. Ajdari, Engineering flows in small devices: Microfluidics toward a lab-on-a-chip, Annu. Rev. Fluid Mech. **36**, 381 (2004).
[3] Y. Tagawa, N. Oudalov, C. W. Visser, I. R. Peters, D. van der Meer, C. Sun, A. Prosperetti, and D. Lohse, Highly Focused Supersonic Microjets, Phys. Rev. X **2**, 031002 (2012).
[4] H. Onuki, Y. Oi, and Y. Tagawa, Microjet Generator for Highly Viscous Fluids, Phys. Rev. Appl. **9**, 014035 (2018).
[5] P. Delrot, M. A. Modestino, F. Gallaire, D. Psaltis, and C. Moser, Inkjet Printing of Viscous Monodisperse Microdroplets by Laser-induced Flow Focusing, Phys. Rev. Appl. **6**, 024003 (2016).
[6] E. Turkoz, S. Kang, L. Deike, and C. B. Arnold, Subthreshold laser jetting via flow-focusing in laser-induced forward transfer, Phys. Rev. Fluids **3**, 082201 (2018).
[7] M. Faraday, Xvii. On a peculiar class of acoustical figures; and on certain forms assumed by groups of particles upon vibrating elastic surfaces, Philos. Trans. R. Soc. Lond. **121**, 299 (1831).
[8] E. Turkoz, R. Fardel, and C. B. Arnold, in *Laser Printing of Functional Materials: 3D Microfabrication, Electronics and Biomedicine* (2018).
[9] C. F. Brasz, C. B. Arnold, H. A. Stone, and J. R. Lister, Early-time free-surface flow driven by adeforming boundary, J. Fluid Mech. **767**, 811 (2015).
[10] S. Douady, Experimental study of the faraday instability, J. Fluid Mech. **221**, 383 (1990).
[11] K. Kumar, Linear theory of faraday instability in viscous liquids, Proc. R. Soc. Lond. A **452**, 1113 (1996).
[12] B. J. Gluckman, C. B. Arnold, and J. P. Gollub, Statistical studies of chaotic wave patterns, Phys. Rev. E **51**, 1128 (1995).
[13] M. S. Brown, N. T. Kattamis, and C. B. Arnold, Time-resolved study of polyimide absorption layers for blister-actuated laser-induced forward transfer, J. Appl. Phys. **107**, 083103 (2010).
[14] M. S. Brown, C. F. Brasz, Y. Ventikos, and C. B. Arnold, Impulsively actuated jets from thin liquid films for high-resolution printing applications, J. Fluid Mech. **709**, 341 (2012).
[15] E. Turkoz, A. Perazzo, H. Kim, H. A. Stone, and C. B. Arnold, Impulsively Induced Jets from Viscoelastic Films for High-resolution Printing, Phys. Rev. Lett. **120**, 074501 (2018).
[16] S. Popinet. An accurate adaptive solver for surface-tension-driven interfacial flows, J. Comput. Phys. **228**, 5838 (2009).
[17] S. Popinet, Numerical models of surface tension, Annu. Rev. Fluid Mech. **50**, 49 (2018).
[18] C. J. Howland, A. Antkowiak, J. R. Castrejón-Pita, S. D. Howison, J. M. Oliver, R. W. Style, and A. A. Castrejón-Pita, It's Harder to Splash on Soft Solids, Phys. Rev. Lett. **117**, 184502 (2016).
[19] L. Deike, W. K. Melville, and S. Popinet, Air entrainment and bubble statistics in breaking waves, J. Fluid Mech. **801**, 91 (2016).
[20] L. Deike, E. Ghabache, G. Liger-Belair, A. K. Das, S. Zaleski, S. Popinet, and T. Séon, Dynamics of jets produced by bursting bubbles, Phys. Rev. Fluids **3**, 013603 (2018).
[21] E. Turkoz, J. M. Lopez-Herrera, J. Eggers, C. B. Arnold, and L. Deike, Axisymmetric simulation of viscoelastic filament thinning with the Oldroyd-b model, J. Fluid Mech. **851**, R2 (2018).
[22] C. F. Brasz, J. H. Yang, and C. B. Arnold, Tilting of adjacent laser-induced liquid jets, Microfluid. Nanofluidics **18**, 185 (2015).
[23] N. T. Kattamis, M. S. Brown, and C. B. Arnold, Finite element analysis of blister formation in laser-induced forward transfer, J. Mater. Res. **26**, 2438 (2011).
[24] H. A. Stone, Dynamics of drop deformation and breakup in viscous fluids, Annu. Rev. Fluid Mech. **26**, 65 (1994).
[25] C.-Y. Lai, J. Eggers, and L. Deike, Bubble Bursting: Universal Cavity and Jet Profiles, Phys. Rev. Lett. **121**, 144501 (2018).
[26] S. Douady and S. Fauve, Pattern selection in faraday instability, Europhys. Lett. **6**, 221 (1988).
[27] W. S. Edwards and S. Fauve, Patterns and quasi-patterns in the faraday experiment, J. Fluid Mech. **278**, 123 (1994).
[28] J. W. Miles, Surface-wave damping in closed basins, Proc. R. Soc. Lond. A Math. Phys. Sci. **297**, 459 (1967).
[29] L. Deike, M. Berhanu, and E. Falcon, Decay of capillary wave turbulence, Phys. Rev. E **85**, 066311 (2012).
[30] S. Kumar, Mechanism for the faraday instability in viscous liquids, Phys. Rev. E **62**, 1416 (2000).
[31] I. R. Peters, Y. Tagawa, N. Oudalov, C. Sun, A. Prosperetti, D. Lohse, and D. van der Meer, Highly focused supersonic microjets: Numerical simulations, J. Fluid Mech. **719**, 587 (2013).